

Journal of Geophysical Research: Oceans

RESEARCH ARTICLE

10.1002/2015JC011246

Key Points:

- Shoreline water level is elevated by setup at low tide and SS waves at high tide
- IG waves elevate shoreline water level at all tide stages
- The geomorphic window on Fatato Island is open for 71% of the time

Supporting Information:

- Supporting Information S1

Correspondence to:

E. Beetham,
e.beetham@auckland.ac.nz

Citation:

Beetham, E., P. S. Kench, J. O'Callaghan, and S. Popinet (2016), Wave transformation and shoreline water level on Funafuti Atoll, Tuvalu, *J. Geophys. Res. Oceans*, 121, 311–326, doi:10.1002/2015JC011246.

Received 17 AUG 2015

Accepted 14 DEC 2015

Accepted article online 18 DEC 2015

Published online 10 JAN 2016

Wave transformation and shoreline water level on Funafuti Atoll, Tuvalu

Edward Beetham¹, Paul S. Kench¹, Joanne O'Callaghan², and Stéphane Popinet³

¹School of Environment, University of Auckland, Auckland, New Zealand, ²National Institute of Water and Atmospheric Research, Greta Point, Wellington, New Zealand, ³Sorbonne Universités, UPMC Univ Paris 06, CNRS, UMR 7190 Institut Jean Le Rond d'Alembert, Paris, France

Abstract The influence of sea swell (SS) waves, infragravity (IG) waves, and wave setup on maximum runup (R_{max}) is investigated across different tidal stages on Fatato Island, Funafuti Atoll, Tuvalu. Field results illustrate that SS waves are tidally modulated at the shoreline, with comparatively greater wave attenuation and setup occurring at low tide versus high tide. A shoreward increase in IG wave height is observed across the 100 m wide reef flat at all tidal elevations, with no tidal modulation of IG wave height at the reef flat or island shoreline. A 1-D shock-capturing Green-Naghdi solver is used to replicate the field deployment and analyze R_{max} . Model outputs for SS wave height, IG wave height and setup at the shoreline match field results with model skill >0.96. Model outputs for R_{max} are used to identify the temporal window when geomorphic activity can occur on the beach face. During periods of moderate swell energy, waves can impact the beach face at spring low tide, due to a combination of wave setup and strong IG wave activity. Under mean wave conditions, the combined influence of setup, IG waves and SS waves results in interaction with island sediment at midtide. At high tide, SS and IG waves directly impact the beach face. Overall, wave activity is present on the beach face for 71% of the study period, a significantly longer duration than is calculated using mean water level and topographic data.

1. Introduction

The cause of inundation on atoll islands is commonly linked to extreme spring tides that can submerge low lying areas on sedimentary reef landforms [Lin et al., 2014; Woodroffe, 2008; Yamano et al., 2007]. However, recent research has predicted that wave overtopping will become the most frequent cause of island flooding as sea levels rise [Hoeke et al., 2013; Merrifield et al., 2014]. Runup generated from distant source swell waves or locally generated storm waves can overtop and flood atoll islands; causing significant damage to infrastructure [Ford et al., 2013; Hoeke et al., 2013; Shimozono et al., 2015]. Notwithstanding the concerns raised by such episodic events, geomorphic change can also occur under nonextreme conditions when waves interact with sediment on the beach face [Kench and Brander, 2006]. To date, few studies have examined the temporal exposure of reef island shorelines to different frequency wave processes.

Shoreline water level on atoll reefs is primarily influenced by sea swell (SS) waves, infragravity waves (IG), wave setup, and tidal elevation [Merrifield et al., 2014]. Incident SS wave energy (>0.04 Hz) is dissipated through wave breaking at the reef edge and by friction across the reef flat [Hearn, 1999; Péquignet et al., 2011]. Field experiments have demonstrated a strong tidal control on SS wave transmission across the reef, with attenuation between 70% (high tide) and 100% (low tide) [Ford et al., 2013; Kench and Brander, 2006; Péquignet et al., 2011]. Consequently, field results indicate that the potential for SS wave driven geomorphic change at the island shoreline is typically constrained to high tide [Brander et al., 2004; Kench and Brander, 2006]. Despite these findings, few studies have extended the analysis of wave transformation beyond a near shoreline instrument to include runup limits on the beach face.

IG frequency waves (<0.04 Hz) are released when SS waves interact with the reef edge [Péquignet et al., 2014; Pomeroy et al., 2012]. Field measurements across narrow atoll reefs (~100 m) indicate that IG waves contribute the main form of shoreline energy under mean and swell wave conditions [Ford et al., 2013]. A long period swell event propagated across the Pacific Ocean in December 2008 and resulted in runup at IG frequencies that caused inundation across a series of Pacific Island nations [Hoeke et al., 2013]. However, measurements on wide fringing

reefs indicate that IG waves generated under mean wave conditions will peak near the reef edge (~ 100 m) and be dissipated by friction across the reef flat [Péquignet et al., 2014; Pomeroy et al., 2012; Van Dongeren et al., 2013]. Numerical analysis of wave transformation under extreme typhoon conditions shows that damaging IG waves can impact the shoreline on wide and shallow fringing reefs [Shimozono et al., 2015]. Wave breaking at the reef edge also generates a setup water level across the reef flat [Gourlay, 1996]. On average, setup on coral reefs has been measured to be 25% of incident H_s [Jago et al., 2007; Vetter et al., 2010]. However, Becker et al. [2014] identify a strong tidal control; with maximum setup at low tide exceeding 40% of incident H_s , and a relatively small setup at high tide ($< 10\%$ of H_s). Large setup results in less attenuation from friction on the reef flat, allowing larger wave heights at the shoreline and an elevated point of interaction for SS and IG waves on the beach face.

Recent research on wave transformation across atoll reefs has focused on wave overtopping [Hoeke et al., 2013; Merrifield et al., 2014; Quataert et al., 2015], without considering the processes that promote wave activity on the beach face. Sea level, tidal oscillations, setup, IG waves, and SS waves combine to determine reef flat water level and the point of maximum runup at the shoreline [Merrifield et al., 2014]. In turn, reef flat water level and runup influence the temporal window for geomorphic activity on sedimentary islands. Therefore, it is necessary to investigate wave transformation in the context of the processes that impact shoreline water level in order to understand the key drivers of geomorphic change on atoll landforms.

This research considers how SS waves, IG waves, and wave setup influence shoreline water level on atoll islands. Wave transformation data are presented from field measurements taken over a 62 day period on Funafuti Atoll. Funafuti is often cited as being especially vulnerable to sea level rise, with spring tides regularly flooding island infrastructure [Lin et al., 2014; Yamano et al., 2007]. Analysis of sea level data from the last 60 years shows that Funafuti is currently experiencing a rise in mean sea level of 5.1 mm/yr, 3 times the global average [Becker et al., 2012]. Despite this highlighted vulnerability, no attempt has been made to quantify the wave processes that impact island shorelines on Funafuti Atoll. Field results are presented first to understand how tide level and incident wave conditions influence SS waves, IG waves, and setup on the reef flat. A fully nonlinear Boussinesq (Green Naghdi) model is then used to replicate field conditions and estimate maximum wave runup at the shoreline. Model results for maximum runup are deconstructed to understand the influence that SS waves, IG waves, and setup have on elevating water level at the shoreline. A thorough review of model performance and sensitivity is presented before numerical results are used to extend field measurements from a near shoreline instrument to the runup limit.

2. Field Setting

Field data were collected on the ocean-facing reef flat near Fatato Island on Funafuti Atoll, Tuvalu. Fatato is an uninhabited island, 87 m wide and 860 m long, composed of coarse coral gravel. The island is located on a 300 m wide reef flat with an ocean side reef width of 100 m and an average fore-reef slope of 23.5° (Figure 1). A discontinuous cemented rubble bank is located on the inner reef flat (Figure 1d). The cemented bank is the remains of a rubble rampart that was deposited 30 m from the reef edge during Tropical Cyclone Bebe in October 1972 [Maragos and Beveridge, 1973]. A ~10 m wide conglomerate platform is located between the area of cemented rubble and the beach face, with the seaward edge 0.3 m below mean sea level (MSL). The island beach is located from 0.39 m above MSL and forms a steep beach face (12.2°), with a berm elevated 3.5 m above MSL (Figure 1d). Sediment on the ocean-facing beach is predominantly gravel sized (-4.2 to -6.4 phi) with some sand sized sediment from 1.15 to -0.32 phi [Ryan, 2012]. Fatato Island is located on the south-east side of Funafuti, facing 143° and is directly exposed to waves approaching between 60° and 213°. Mean H_s near Funafuti is 1.2 m in summer and 1.4 m in winter (30 year Wave Watch 3 data), with mean peak direction (D_p) shifting from 145° in summer to 135° in winter [Durrant et al., 2014].

3. Methodology

3.1. Field Campaign

3.1.1. Wave Data

Over a 62 day field deployment waves were measured by three separate wave and tide instruments located: offshore, on the outer reef flat, and near the island shoreline (Figure 1d). The instruments were deployed to record pressure (water level) at 1 Hz for 2048 s (~ 34 min) every 3 h. Data collection started at 12 pm on 4 June 2013 and ended at 9 pm on 5 August 2013, resulting in 500 synchronized bursts. In order to measure

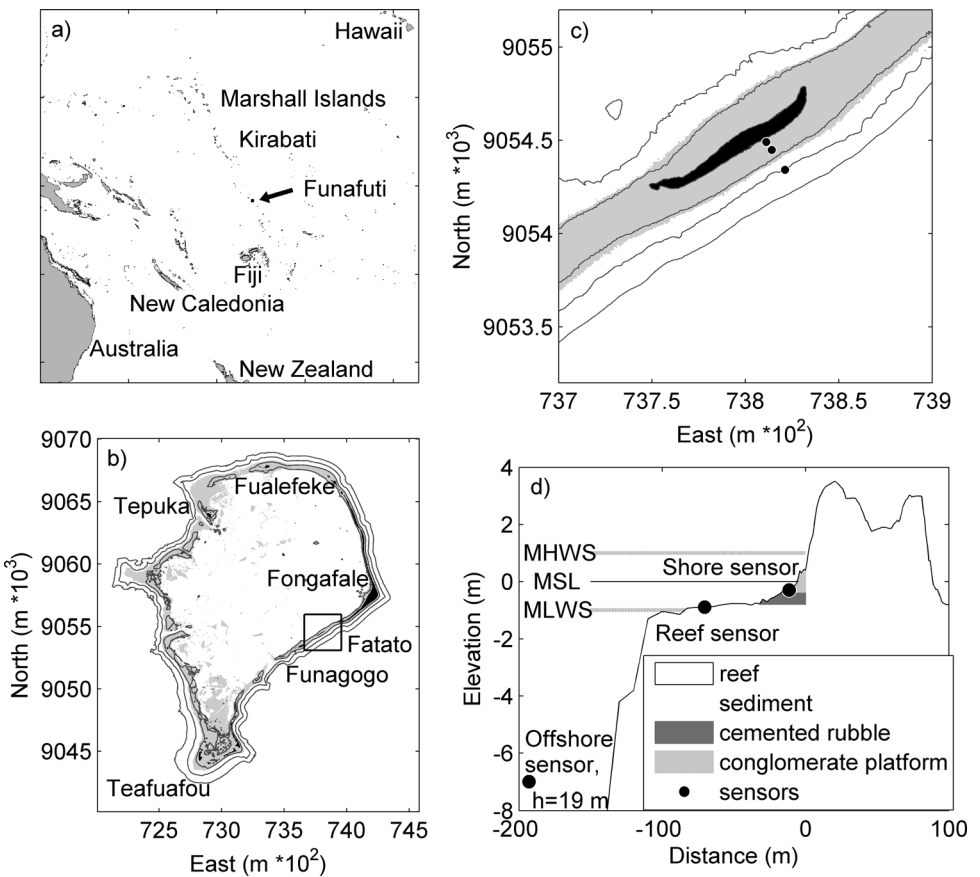


Figure 1. (a) Location of Funafuti Atoll in the Pacific Ocean. (b) Funafuti Atoll with contour lines at -500 , -200 , and -2 m, islands are black and the reef flat ($h > 3$ m) is grey. (c) Bathymetry around Fatato Island with field instrument positions and contours at -100 , -20 , and -2 m. (d) Profile of the reef flat and Fatato Island, highlighting geomorphic features, and instrument locations.

incident waves, a Nortek AWAC was deployed at a depth of 19 m on the fore-reef slope. In addition, two RBR Tide and Wave recorders (TWRs) were deployed on the reef flat. The outer reef flat TWR was deployed 70.4 m seaward of the island beach (32 m shoreward of the reef edge) at an average depth of 0.9 m below MSL. The shoreline TWR was positioned at the seaward edge of the conglomerate platform (MSL—0.38 m); 11.6 m seaward of the beach toe (Figure 1d). Both TWRs were bolted to the reef with sensors 0.05 m above the bed.

Pressure data from the AWAC were corrected for signal attenuation using the method described in *Tucker and Pitt* [2001]. Following *Ford et al.* [2013] and *Pomeroy et al.* [2012] a 0.04 Hz spectral band-pass filter was used to separate water level oscillations into SS and IG frequencies before calculating wave statistics. Significant wave height and period associated with SS (H_{ss} , T_s) and IG (H_{ig} , T_{ig}) waves were then calculated using the zero-downcrossing method. Power spectral density was calculated from the unfiltered water level data using a Fast Fourier Transform with 8 degrees of freedom and an overlapping Hamming window [Welch, 1967]. Wave setup ($\bar{\eta}_i$) at each reef flat sensor was calculated by identifying the difference in mean depth between the reef sensor and the offshore sensor, relative to the difference in topographic elevation:

$$\bar{\eta}_i = \bar{h}_i - (\bar{h}_o + \Delta h_i), \quad (1)$$

where \bar{h}_i is the burst average depth at the reef flat sensor, \bar{h}_o is the burst average water depth at the offshore sensor, and Δh_i is the difference in elevation between the offshore sensor and the reef flat ($\Delta h = 18.33$) and shoreline ($\Delta h = 18.82$) sensors. This method assumes no setup or set-down at the offshore sensor.

3.1.2. Topography

A laser level total station was used to measure reef and island topography on 10 across reef transects; including the instrument profile. The profiles were combined with RTK-GPS survey points from the reef flat to create a terrain model of the reef flat and shoreline. This shallow water topography data were combined with satellite imagery and

single beam echo-sounding data from Hoeke *et al.* [2014] to create a bathymetry map of the atoll reef flat near Fatato Island (Figure 1c). All references to topography used in field and model analysis are relative to MSL = 0.

3.2. Green-Naghdi Model

Field conditions were simulated using a Green-Naghdi free-surface solver from the open source model, Basilisk [Popinet, 2015]. The GN solver extends the nonlinear shallow water (NSW) solver from Popinet [2011] to include a weakly dispersive source term for wave propagation and shoaling. The combination of GN and NSW terms has been proven to provide an efficient solution of wave dispersion, wave breaking, and wet-dry interaction in shallow coastal environments [Bonneton *et al.*, 2011; Lannes and Marche, 2015; Tissier *et al.*, 2012]. In 1-D, the Basilisk GN solver has been verified against benchmark data for: solitary wave runup on a plain beach, solitary wave overtopping a sea wall, and wave propagation over a bar [Popinet, 2014]. In 2-D, the model has been successfully tested against benchmark data for: wave propagation over an ellipsoid shoal, solitary wave runup on a conical island, and tsunami propagation and runup from the Tohoku earthquake [Popinet, 2015].

3.2.1. Numerical Scheme

A brief outline of the Basilisk GN model is given here. The reader is encouraged to refer to Popinet [2015] for a full description, or the Basilisk website for the documented source code [Popinet, 2014].

In integral form, the GN equation set is:

$$\partial_t \int_{\Omega} \mathbf{q} d\Omega = \int_{\partial\Omega} \mathbf{f}(\mathbf{q}) \cdot \mathbf{n} d\partial\Omega + \int_{\Omega} \mathbf{S} d\Omega \quad (2)$$

where $\partial\Omega$ is the boundary and \mathbf{n} is the unit normal vector of a given subset of space, Ω . For conservation of mass and momentum in shallow water, \mathbf{q} and $\mathbf{f}(\mathbf{q})$ are from the NSW system outlined in Popinet [2011], and are written as:

$$\mathbf{q} = \begin{pmatrix} h \\ h u_x \\ h u_y \end{pmatrix}, \quad \mathbf{f}(\mathbf{q}) = \begin{pmatrix} h u_x & h u_y \\ h u_x^2 + \frac{1}{2}gh^2 & h u_x u_y \\ h u_x u_y & h u_y^2 + \frac{1}{2}gh^2 \end{pmatrix} \quad (3)$$

where u is the velocity vector and h is water depth.

The weakly dispersive source term in (2) is \mathbf{S} , defined as:

$$\mathbf{S} = \begin{pmatrix} 0 \\ -hg\nabla z_b + h\left(\frac{g}{\alpha}\nabla\eta - \mathbf{D}\right) \end{pmatrix} \quad (4)$$

where z_b is bathymetry elevation, η is free surface elevation, and α is a dispersion constant with the default value of 1.153. The second part of (4), $h((g/\alpha)\nabla\eta - \mathbf{D})$, is the dispersive term that is added to the original NSW system [Popinet, 2015]. If this second term is removed or equal to zero the system reduces to a nondispersive NSW model.

3.2.2. Wave Breaking

Wave breaking is represented by switching off the dispersive source term if the local free-surface slope ($\|\nabla\eta\|$) exceeds a user-defined breaking threshold (B); by default $B = 1$. Removing the dispersive term refers the model to a NSW system, where wave breaking is handled as a shock [Popinet, 2015]. Similar methods for wave breaking in Boussinesq-type models have been successfully applied to coral reef environments [Roeber and Cheung, 2012; Shimozono *et al.*, 2015]. The dispersion term is also removed if a cell has a “dry” neighbor (where $h < 10^{-10}$ m is considered dry). Therefore, wet-dry interaction is handled by the NSW equations that include a hydrostatic reconstruction technique from Audusse *et al.* [2004] to guarantee positivity of water depth [Popinet, 2011, 2012]. For the simulations presented here, implicit quadratic bottom friction was added to equation (4) in the form of (5):

$$\mathbf{S}_f = -C_f \|\mathbf{u}\| \mathbf{u} \quad (5)$$

where C_f is a nondimensional coefficient that controls the rate of attenuation. A constant C_f value was used across the model domain for the simulations presented here.

3.3. Model Experiments

Sensitivity analysis was undertaken to identify the appropriate C_f and B values to use on Funafuti. Four B slopes (0.4, 0.6, 0.8, and 1) and 8 C_f values (0.01, 0.02, 0.03, 0.04, 0.05, 0.06, 0.08, and 0.1) were tested using 10% of the field data (50 bursts). Each B value was simulated with each C_f value using the 50 test bursts; a total of 1600 simulations. The 50 consecutive bursts used to test model sensitivity encompassed a range of incident conditions between 23 June and 29 June 2013, and notably included a swell event that coincided with spring tides. Model outputs for H_{ss} , H_{ig} , and $\bar{\eta}$ at the shoreline were compared with field measurements to identify the C_f and B combination that best represents conditions on Funafuti. All 500 bursts from the field campaign were then simulated using the B and C_f combination that produced the lowest combined error for H_{ss} , H_{ig} , and $\bar{\eta}$ at the shoreline. Model outputs for H_{ss} , H_{ig} , $\bar{\eta}$, and wave spectra from the 500 bursts were then compared with field data at the reef flat and shoreline, before model outputs were used to analyze maximum water level on the beach face.

3.3.1. Model Inputs

Measured water level from the offshore instrument was interpolated to 10 Hz to use as the boundary wavefield for each simulation (supporting information Figure S1a). The Basilisk GN solver was used with a 1-D grid to simulate wave transformation across the atoll reef. Reef bathymetry was interpolated to a uniform 1-D transect with $\Delta x = 1$ m, and still water level was offset according to the tide level of each burst. To reduce boundary reflection, imported waves were propagated across a flat shelf (100 m deep) for 650 m before interacting with the atoll reef slope (supporting information Figure S1b). Wave statistics were calculated at the AWAC location to make sure the model wavefield matched field measurements.

3.3.2. Output Data Analysis

Each test burst simulated 2048 s of wave activity. It took ~ 100 s for waves to reach the shoreline and ~ 300 s for mean water level to stabilize on the reef. Therefore, only output data between 512 and 2048 s was considered for analysis. To compare model results with field results, time series water level was extracted at 10 Hz, at each of the three instrument positions (Figure 1d). H_{ss} , H_{ig} , $\bar{\eta}$, and wave spectra were calculated from each model instrument using the same methods applied to field data.

3.3.3. Maximum Runup Analysis

Maximum water level data were extracted at the end of each model run and used to identify maximum wave runup (R_{max}) for each simulation. Of note, field data were unable to be collected for runup and all R_{max} results are based on model outputs. R_{max} was calculated relative to the still water tide level and then separated into SS, IG, and setup components using model data for H_{ss} , H_{ig} , and $\bar{\eta}$ from the shoreline field instrument position (Figure 1d). First, the difference between tide level and R_{max} was calculated. Second, the setup contribution was identified (equal to $\bar{\eta}$ at the shoreline), and subtracted to determine the combined SS and IG contribution. The remaining R_{max} value was split into SS and IG components proportional to the values of H_{ss} and H_{ig} at the shoreline. Note, this method calculates maximum runup to the nearest horizontal meter ($\Delta x = 1$ m) and does not account for the influence that wave period has on swash elevation.

3.3.4. Performance Metrics

Mean absolute error (MAE) and model skill were used to quantify model performance when predicting H_{ss} , H_{ig} , and $\bar{\eta}$. MAE (6) and skill (7) are based on residual values where the observed value (O_i) was subtracted from modeled value (P_i). Model skill is based on the method used in Lowe *et al.* [2009]. Skill is equal to one when $P_i = O_i$, meaning skill values closer to one identify a better representation of measured processes.

$$MAE = |P_i - O_i| \quad (6)$$

$$Skill = 1 - \frac{\sum |(P_i - O_i)|^2}{\sum (|P_i - \bar{O}| + |O_i - \bar{O}|)^2} \quad (7)$$

4. Field Observations

4.1. Tide and Wave Conditions

Two semidiurnal spring tides were recorded during the 62 day data collection period. A spring tidal range of ~ 2 m was observed, where the maximum high tide was $+1.08$ m relative to MSL = 0, and the minimum low tide was -1.0 m, relative to MSL = 0. Two neap tides were also recorded, with a larger diurnal range between $+0.45$ and -0.35 m and a lower semidiurnal oscillation (Figure 2a). On average, offshore significant wave height (H_o) was 1.17 m, and H_{max} was 2.0 m (Figures 2c, 2d and supporting information Table S1).

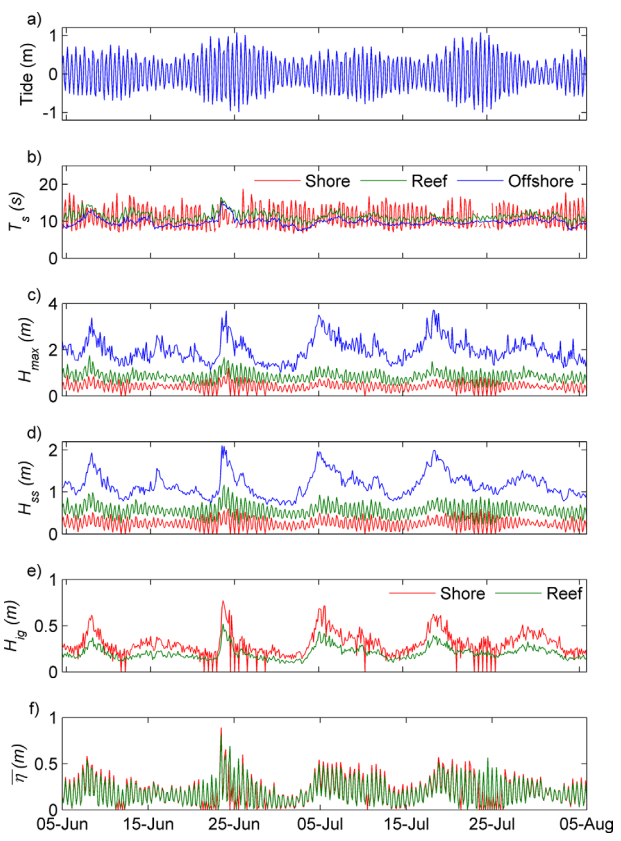


Figure 2. Summary wave conditions from the offshore instrument (blue), reef flat instrument (green), and shoreline instrument (red) from the 62 day deployment in 2013. H_{ss} and H_{ig} are significant wave heights in the SS and IG band, respectively. $\bar{\eta}$ is wave setup.

the shoreline. Results show that H_{ss} was tidally modulated across all incident heights. Average attenuation was again greater at low tides (90%), compared to mid (80%) and high (64.5%) tides. Wave height was smallest at low tide (mean = 0.12 m), with 20 bursts recording no wave activity. Larger incident waves (>1.5 m) exhibited less attenuation at low tide, but were significantly attenuated at high tide (Figure 3g). In comparison, smaller incident waves (<1.5 m) were rapidly attenuated at low tide but underwent minimal dissipation at high tide.

Wave periods at the outer reef flat were similar to incident waves, but wave periods at the shoreline observed consistent tidal modulation (Figure 2b). Longer wave periods were observed at low tide (10–17 s) compared to high tides (7–10 s). This indicates that high-frequency waves are filtered out across the reef flat low tide. A shoreline decrease in period at high tides may be a result of incident waves decoupling into higher frequency oscillations on the reef flat.

4.2.2. IG Waves

At the outer reef, H_{ig} was primarily controlled by incident waves and only minimally affected by the tide (Figure 3c). On average, H_{ig} at the outer reef ranged from 10% to 29% of H_o (mean = 17%). H_{ig} increased across the reef flat, and at the shoreline, mean H_{ig} was 25% of H_o . At the shoreline there was a slight tidal influence on small IG waves ($H_{ig} < 0.5$ m); with the largest IG waves observed at midtide (Figure 3h). At low tide H_{ig} was smaller; possibly due to higher friction on the shallow reef flat. At high tide H_{ig} was also relatively smaller; perhaps as a result of decreased SS wave breaking and attenuation. During large incident conditions, results show that H_{ig} was not tidally modulated and was often larger than H_{ss} at the shoreline (Figure 3).

4.2.3. Wave Setup

Mean setup was 0.18 m (16% of H_o) at the outer reef and at the shoreline (supporting information Table S1). Setup at the outer reef was greater at low tide, with a mean of 0.32 m (26% of H_o). At high tide, mean setup on

Four moderate swell events were measured during the deployment (where $H_o \geq 1.9$ m and $T_s > 10.5$ s). The largest swell event started on 23 June and peaked at $H_o = 2.1$ m; with $H_{max} = 3.7$ m and $T_s = 15.5$ s. The swell arrived during a spring tide, with a number of bursts coinciding with spring high tide. Between swell events H_o occasionally dropped below 1 m but remained above 0.68 m (Figure 2).

4.2. Wave Transformation

4.2.1. Sea Swell Waves

On average, incident wave height decreased by 50% between the offshore instrument and the outer reef. On the reef flat, wave height was tidally modulated, especially under low and moderate incident wave conditions (Figure 3a). Mean attenuation was lowest at high tide (35%) compared to mid (51%) and low tides (65%). All bursts recorded wave activity at the outer reef flat; with H_{ss} falling between a minimum of 0.22 m and a maximum of 1.17 m (mean = 0.56 m, supporting information Table S1).

H_{ss} was significantly lower at the shoreline compared to the reef flat; with a mean of 0.25 m and a range of 0–0.61 m. On average, offshore waves attenuated by 78% at

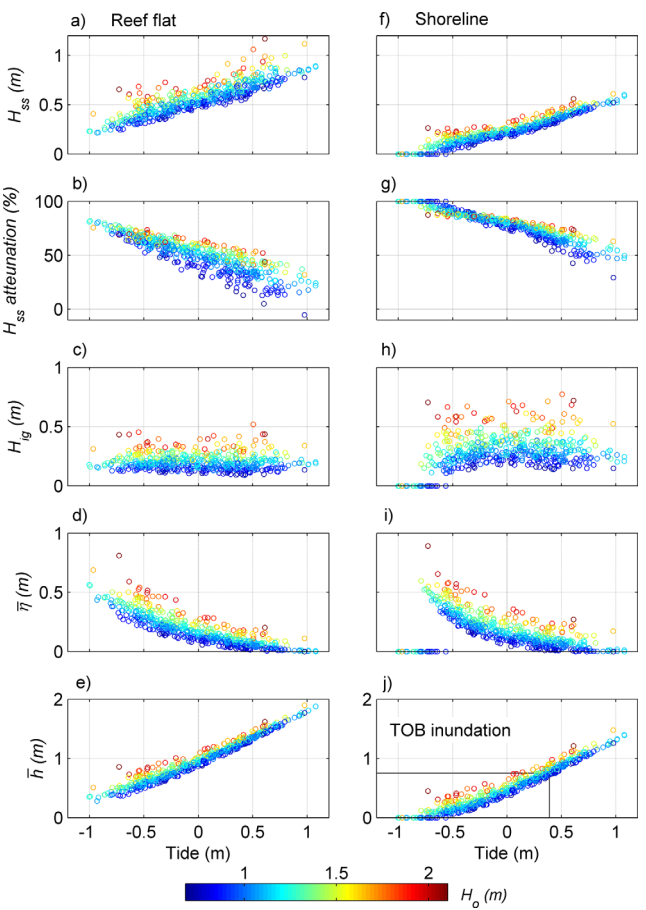


Figure 3. (left) Tidal controls on wave processes on the reef flat and (right) at the shoreline from field measurements. Tide is relative to MSL = 0, η is wave setup and \bar{h} is mean depth (tide + setup). (j) Points outside the small box show that mean depth is above the beach toe (MSL + 0.39 m).

the field deployment period. However, this figure does not account for runup above still water level caused by SS or IG waves. The connection between wave processes and island sediment is further investigated numerically based on maximum runup outputs.

5. Model Results

5.1. Sensitivity to Breaking and Friction Parameters

Modeled wave heights at the shoreline were sensitive to changes in C_f (friction coefficient) and B (slope threshold used to turn off the dispersive term to handle wave breaking using the NSW equations). Lower C_f values (<0.03) resulted in an over-predicted shoreline wave height; with mean error between 0.03 and 0.057 m (Figure 4). Higher C_f (>0.06) resulted in under-predicted shoreline wave heights, with mean error between 0.04 m and 0.06 m (supporting information Figure S2). The lowest error was found with $C_f = 0.04$. Each friction value had a stronger correlation and lower error with $B = 0.8$ or $B = 1$. Lower B values (0.6 and 0.4) often resulted in slightly over predicted wave heights at high tide. The lowest mean error (0.02 m), highest model skill (0.994), and strongest correlation ($R^2 = 0.985$) was achieved using $C_f = 0.04$ and $B = 1$ (Figure 4).

IG wave height was more sensitive to C_f and B values. Lower friction values resulted in significantly over-predicted H_{ig} at the shoreline, with mean error between 0.06 m and 0.15 m for $C_f \leq 0.02$ (Figure 4). $C_f > 0.06$ resulted in under predicted IG wave heights with mean error between 0.07 and 0.12 m (supporting information Figure S2). Higher B values (0.8 and 1) gave a much better prediction of field conditions compared to

the reef flat was 0.07 m (6% of H_o). Mean setup at the shoreline was 0.3 m at low tide, inclusive of the 20 bursts that recorded no wave activity. Wave setup at the reef and shoreline was strongly correlated to tidal level and incident wave height, with maximum setup generated by large waves at low tide (Figure 3). The largest setup observed during the deployment was 0.81 m (38.6% of H_o) at the outer reef and 0.89 m (42% of H_o) at the shoreline. This observation was associated with $H_o = 2.1$ m and $T_o = 15.5$ s at low tide (-0.73 m) at the peak of the 23 June swell event.

4.3. Shoreline Exposure

The island beach was situated 0.39 m above MSL. Consequently, waves could directly interact with the beach face when the tide exceeded $+0.39$ m. From the offshore instrument, it is apparent that tidal elevation exceeded 0.39 m on 112 of the 500 bursts (22.4% of the experiment period). The shoreline instrument was located 0.77 m below the beach face. Mean depth at the shoreline instrument (tide + setup) exceeded 0.77 m on 125 of the 500 bursts (25% of the experiment period). This data suggests that any interaction between oceanic processes and the beach face was confined to 25% of

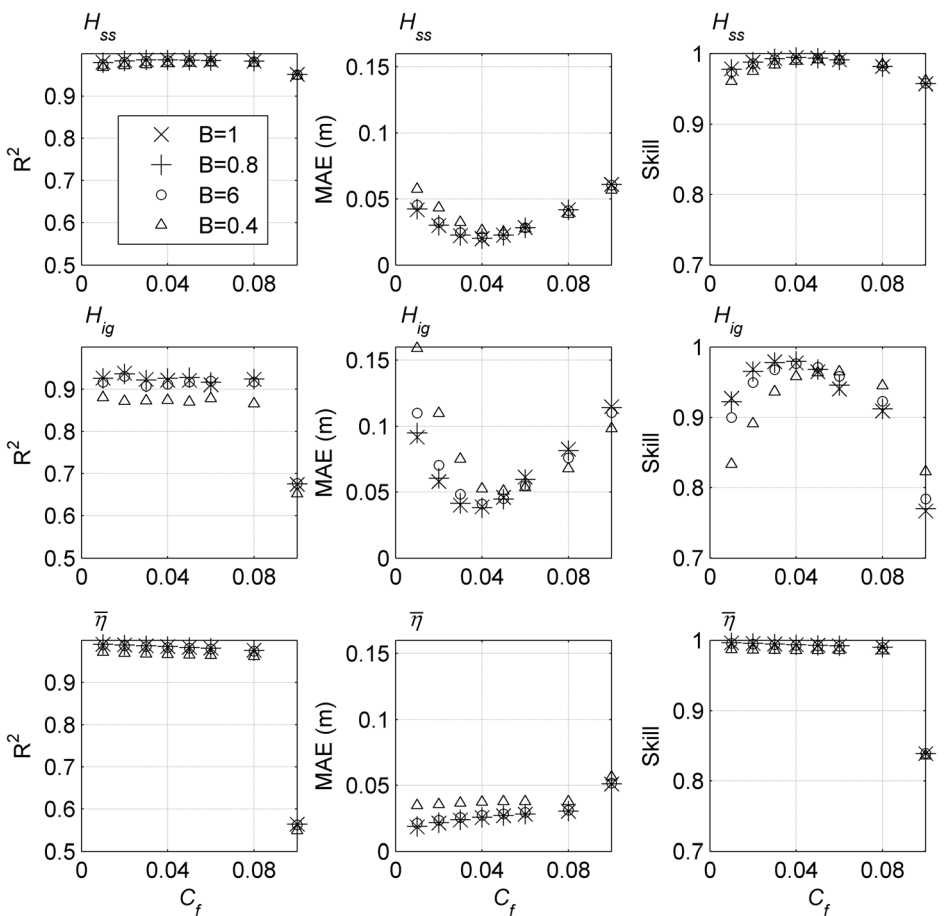


Figure 4. Sensitivity of modeled H_{ss} (top), H_{ig} (middle), and $\bar{\eta}$ (bottom) at the shoreline, to variations in B and C_f . Model performance is quantified using (left) R^2 , (left) MAE, and (right) skill.

low slopes (0.6 and 0.4). The best representation of H_{ig} at the shoreline was achieved using $C_f = 0.04$ and $B \geq 0.8$. IG error was slightly lower with $B = 0.8$ compared to $B = 1$ (Figure 4).

Model values for wave setup were close to field measurements for most B and C_f combinations (supporting information Figure S2). The only deviation from a near perfect prediction was found using $B = 0.4$ or $C_f > 0.06$ (Figure 4). For each friction value, $B = 1$ achieved the best prediction of wave setup. $C_f = 0.01$ and $B = 1$ gave the best representation of wave setup; however any C_f value between 0.01 and 0.05 produced a very good match with field data where $B = 1$ (Figure 4).

5.1.1. Combined Error

The lowest error and highest model skill were achieved using $C_f = 0.04$. When applied to the steep sloping, rough and shallow atoll reef at Funafuti, the model gave the best prediction of H_{ss} , H_{ig} , and $\bar{\eta}$ when a breaking slope of 0.8 or 1 was combined with $C_f = 0.04$. Using $C_f = 0.04$ the sum MAE from H_{ss} , H_{ig} , and $\bar{\eta}$ for both $B = 1$ and $B = 0.8$ was 0.084 m (supporting information Table S2). $B = 1$ gave a better prediction for H_{ss} and setup but $B = 0.8$ gave a slightly better prediction for H_{ig} . However, there was minimal sensitivity between $B = 1$ and $B = 0.8$. Therefore, the values used to simulate the entire field deployment and investigate R_{max} were $C_f = 0.04$ and the default slope threshold, $B = 1$.

5.2. Full Experiment Simulation

5.2.1. Model Performance

A comparison between model outputs and field data for the entire experiment using $C_f = 0.04$ and $B = 1$ is presented in Figure 5. Model performance across the 500 simulations was characterized by Skill > 0.91 , MAE < 0.045 and $R^2 \geq 0.8$, based on outputs for H_{ss} , H_{ig} , and $\bar{\eta}$ at the reef flat and shoreline.

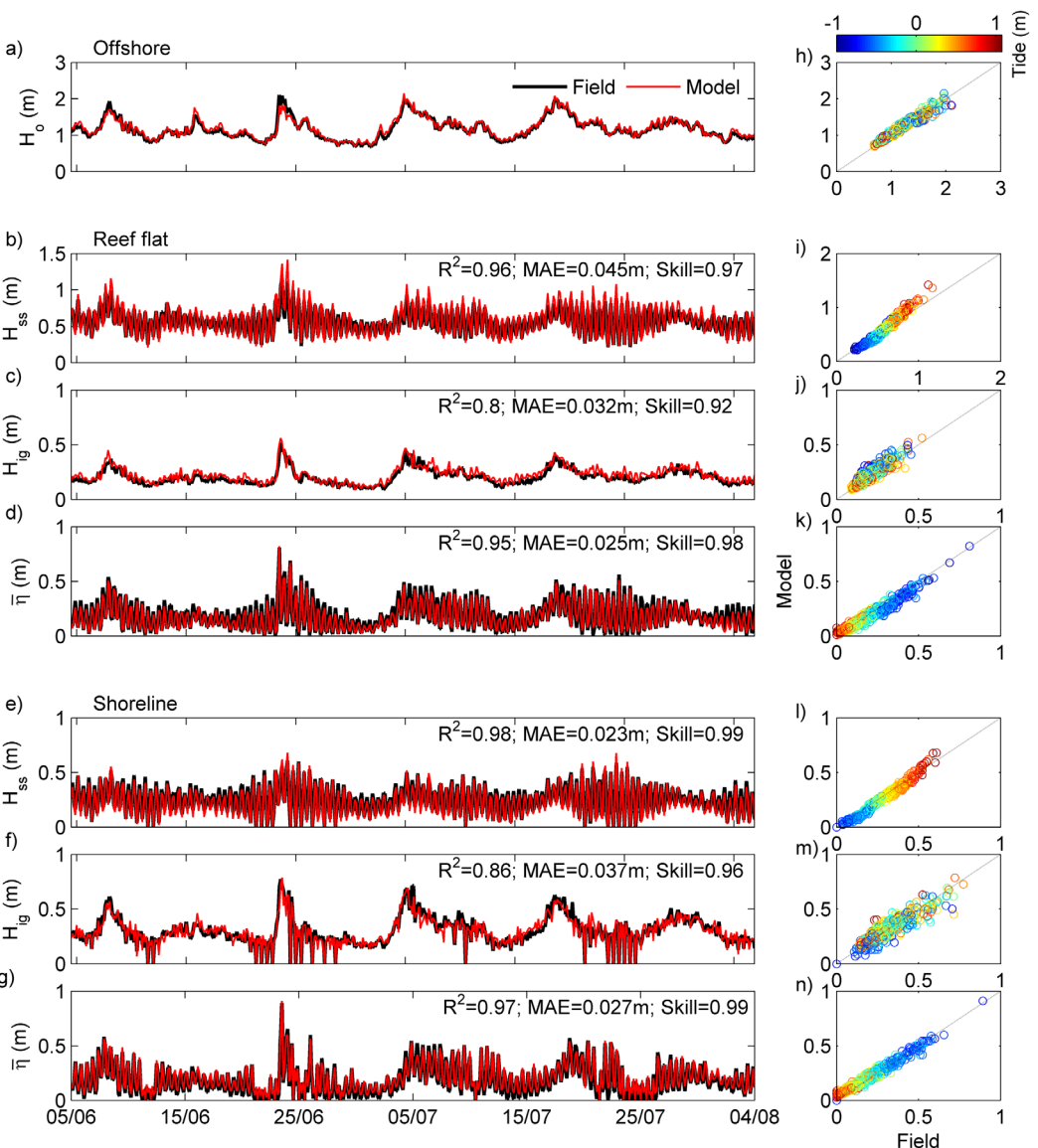


Figure 5. (a–g) Model outputs (red) compared to field measurements (black) for the 62 day experiment. (a) Incident H_o , (d–b) H_{ss} , H_{ig} , and $\bar{\eta}$ at the outer reef and (e–g) at the shoreline. (h–n) The same data from each time series comparison are also presented as a scatter, on the same line.

Field results show that H_{ss} at the reef and shoreline is primarily a function of tide level and incident wave height. The high skill (>0.97) associated with modeled H_{ss} at the reef and shoreline indicate that tidal controls and incident forcing were numerically replicated very well (Figure 5). H_{ss} at the outer reef flat was generally over-predicted (MAE = 0.045 m), especially during energetic conditions (Figure 5i). Modeled H_{ss} at the shoreline had smaller error (MAE = 0.023 m), but the smaller wave heights observed at low tide were slightly under-predicted (Figure 5l).

Model results show the same general pattern as measured H_{ig} at the reef flat and shoreline (Figures 5c and 5f). Numerical simulations also reflect the increase in H_{ig} between the reef flat and shoreline. Compared to H_{ss} and $\bar{\eta}$, model predictions of H_{ig} had greater error, lower skill, and a weaker correlation to field results. The weaker prediction is possibly associated with the observation that IG waves have no pronounced tidal modulation. Despite the deviation from a perfect fit, IG wave dynamics across the reef flat were captured reasonably well in the numerical model (Figure 5).

Modeled wave setup followed the same tidal modulation and relation to H_o as field measurements (Figure 5). Figure 5d shows how the setup peaks at low tide were slightly under-predicted at the reef flat,

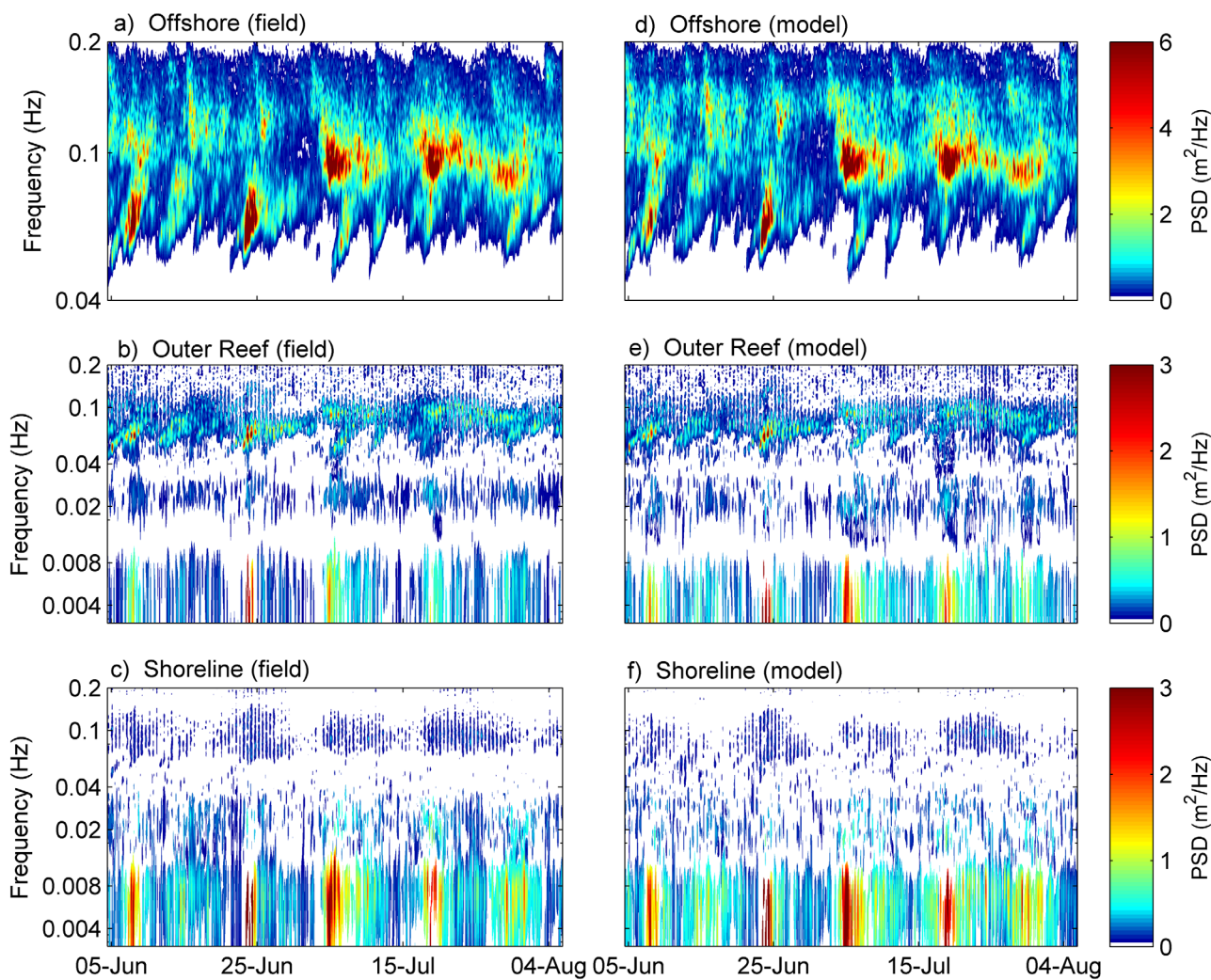


Figure 6. (left) Field wave spectra from the (a) offshore instrument, (b) outer reef flat, and (c) shoreline compared to wave spectra calculated using (right) model outputs at the (d) offshore location, (e) outer reef flat, and (f) shoreline. (a and d) Note, the y axis is a log scale to show more detail within the IG band and offshore spectra have different y axis and z axis (color) limits compared to the reef flat and shoreline plots.

but well predicted at the shoreline. However, the low setup values at high tide were slightly overpredicted at the shoreline (Figure 5g).

5.2.2. Field and Model Wave Spectra

Measured wave data were used to run model simulations. Consequently, at the offshore sensor, model spectra were almost identical to field measurements (Figures 6a and 6d). When averaged across the deployment, field based spectra depicted a bimodal peak in incident wave energy during the study period (supporting information Figure S3). A shorter period peak at 0.094 Hz (10.6 s) was associated with mean wave conditions and the latter two swell events (Figure 6a). A longer period peak at 0.065 Hz (15.4 s) was associated with the first two swell events (Figure 6a). Deployment averaged model spectra illustrated a similar bimodal peak in incident wave spectra (supporting information Figure S3).

On the reef flat, the presence of energy at incident wave frequencies was limited to high tide, with greater spectral density occurring during energetic conditions (Figure 6b). Spectra on the reef flat peaked in the IG band at 0.0049 Hz (204 s), with a secondary peak in the swell frequency band (0.072 Hz) during larger incident conditions (Figure 6b). At the outer reef flat, modeled wave spectra identified a clear IG wave signal. However, peak energy occurred at a lower frequency (0.0037 Hz, 270 s). The presence of swell wave energy on the reef flat at high tide was evident in model spectra, with peak energy at 0.072 Hz; the same as field measurements.

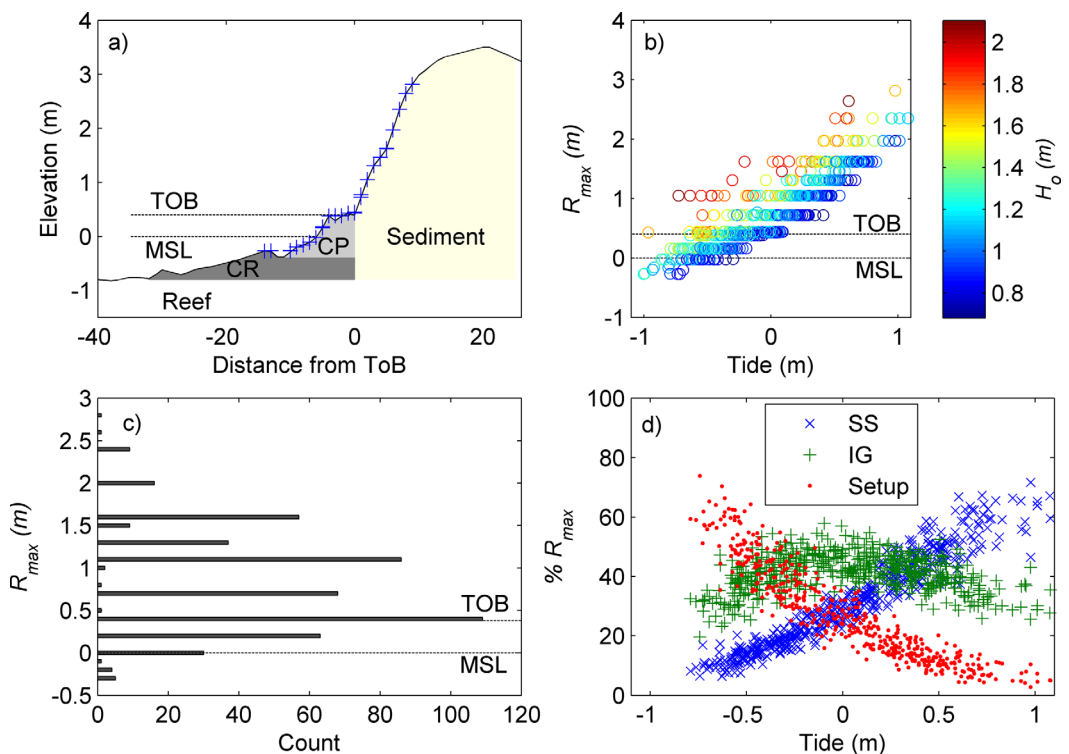


Figure 7. R_{max} analysis using model data. (a) R_{max} location from each burst, highlighting the toe of beach (TOB) threshold for wave interaction with island sediment. (b) Tidal controls on R_{max} above MSL under different incident wave conditions. (c) R_{max} frequency at different elevations, relative to MSL = 0. (d) The contribution of wave setup (dots), IG waves (+), and SS waves (x) in R_{max} above tide level.

Field based spectra demonstrate that SS waves were nearly fully dissipated at the shoreline, with energy concentrated at IG frequencies (Figure 6c). However, some incident frequency energy was present at the shoreline at high tide or during swell events. IG wave energy was present at the shoreline during mean wave conditions at high tide but was amplified throughout the tide cycle when larger incident waves were present. Field data indicate that IG wave energy increased between the reef flat and shoreline where spectral density peaked at 0.0068 Hz (146 s). Modeled spectra at the shoreline showed a similar spectral density to field results, but with a slightly higher peak frequency of 0.0061 Hz (163 s). The over-predicted IG period may be a result of using the model in 1-D, and therefore omitting the alongshore processes that influence long-wave behavior.

5.3. Maximum Runup

The Basilisk GN model was able to replicate water level variations on the reef flat associated with SS waves, IG waves, and wave setup. Combined, these processes influence shoreline water level and the maximum runup point that is reached under a particular set of incident conditions. Model results were analyzed to identify R_{max} for each burst. Across all simulations R_{max} was located between the inner reef flat and upper beach face (Figure 7a). The elevation of R_{max} relative to MSL is primarily a function of incident wave height and tide level (Figure 7b). Large waves at low tide produced an elevated setup and energetic IG waves that resulted in the same runup elevation as small waves at high tide (Figure 7). During 67 bursts (13.4%), R_{max} reached the top of the conglomerate platform and was level with the toe of beach (MSL + 0.39 m). Wave interaction with the midbeach face ($R_{max} > 0.5$ m) occurred during 287 bursts; accounting for 57.4% of the experiment (Figure 7c). Collectively, waves reached or exceeded the beach toe for 70.8% of the experiment (354 bursts). Numerical runup results indicate that the geomorphic window of interaction between waves and island sediment is open for a much longer period of time than was estimated using mean water level.

The combined processes that contribute to R_{max} vary through the tide cycle (Figure 7d). At low tide (< -0.4 m), wave setup is the primary mechanism contributing to shoreline water level. At midtide stages ($-0.4 \text{ m} > +0.3$ m), the influence of setup decreases significantly and IG waves become the dominant contribution to runup level (Figure 7d). As tide level increases there is a linear increase in the portion of runup associated

Table 1. Percentage of R_{max} Associated With SS Waves, IG Waves, and Setup at Different Tide Stages

	High Tide	Midtide	Low Tide	All Tides
SS (%)	48.7	29.2	14.9	31.6
IG (%)	39.3	44.7	38.8	41.0
Setup (%)	12.0	26.1	46.3	27.4

5.3.1. Swell Driven Shoreline Exposure on June 23

The largest waves measured during the field experiment ($H_o = 2.10 \text{ m}$, $T_o = 15\text{s}$) coincided with spring tides on 23 June 2013. The swell event generated significant wave setup and IG activity, and model results indicate the presence of waves on the beach face throughout the tide cycle (Figure 8). The swell peaked at low tide (-0.73 m), when a 0.9 m setup resulted in a mean shoreline depth 0.05 m above MSL (Figure 8a). Model results show that the combined runup from IG and SS waves was able to surge over the conglomerate platform and impact the beach face to an elevation of 1.05 m . Runup was primarily associated with wave setup (51.1%), and IG waves (31.9%), but there was also a small SS wave contribution (17%).

At high tide ($+0.61 \text{ m}$), the swell event generated a runup of 2.03 m above tide level and an R_{max} elevation of 2.64 m above MSL (Figure 8b). The deeper reef flat resulted in significantly less wave setup that accounted for 15% of R_{max} .

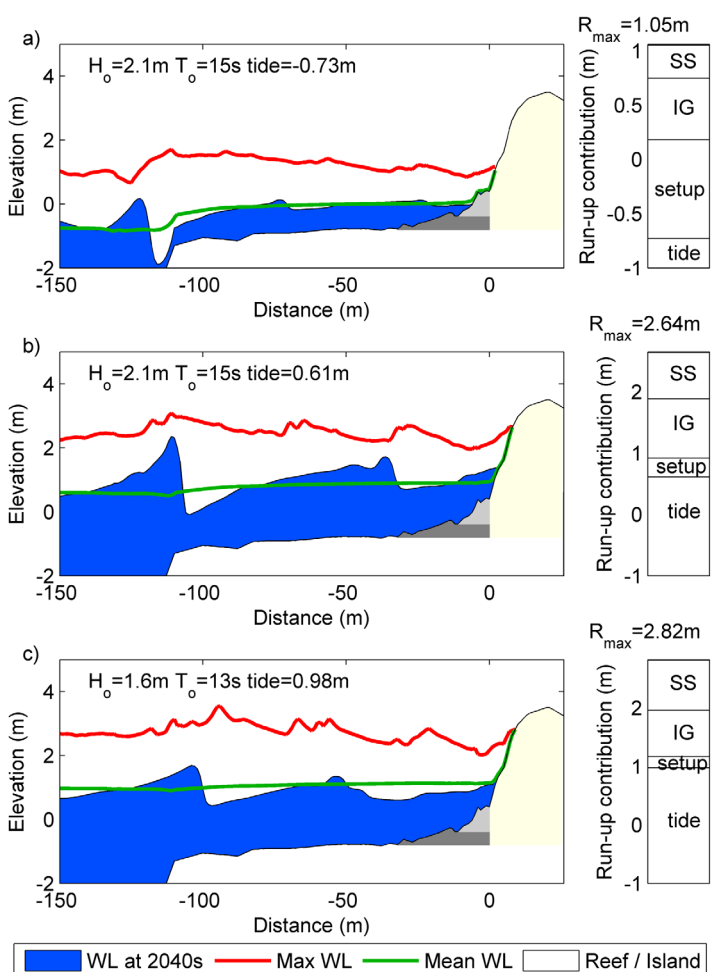


Figure 8. Model outputs for instant, mean and maximum water level (WL) on the reef and shoreline during the spring tide swell on 23 June. (a) Setup dominant R_{max} at low tide. (b) IG dominant R_{max} at high tide. (c) SS dominant R_{max} at high tide. Bar plots on the right highlight the contribution of tide level, setup, IG waves, and SS waves in runup, relative to MSL = 0.

Large IG waves at the shoreline ($H_{ig} = 0.72 \text{ m}$) accounted for 48% of R_{max} and therefore acted as the main control on runup elevation. SS waves were also able to propagate across the reef to account for 37% of R_{max} . The highest runup above MSL occurred during a spring high tide (MSL + 0.98 m), when the swell was decreasing (Figure 8c). The combined influence of setup (10.5%), IG waves (43%), and SS waves (46.5%) resulted in R_{max} 2.82 m above MSL. Note that under large incident conditions waves do reflect off the shoreline at high tide and interfere with the oncoming wavefield, resulting in the maximum water level line from Figures 8b and 8c.

6. Discussion

6.1. Tidal Modulation of Reef Flat Processes

Field observations from Funafuti show that H_{ss} is strongly modulated by water depth across the reef, a function of tide level and setup (Figure 3). Tidal modulation of shoreline wave height has been well documented on a

range of fringing, atoll, and platform reefs [Ford *et al.*, 2013; Kench and Brander, 2006; Lugo-Fernandez *et al.*, 1998; Péquignet *et al.*, 2011]. The majority of these studies present a strong relationship between wave height and mean reef depth, concluding that SS activity at the shoreline is limited to high tide. Few studies have recorded shoreline wave activity at low tide. Field results from Funafuti emphasize how large setup at low tide can submerge the reef flat and enhance the potential for waves to impact the shoreline throughout the tidal cycle. Compared to other field studies, the narrow reef and consistent exposure to moderate or high energy waves create a relatively active shoreline wave regime. As a result, SS and IG waves are almost always present at the shoreline during low and high tide.

Tidal modulation of wave setup has been identified on coral reefs [Becker *et al.*, 2014; Gourlay, 1996]. The results from this study support observations of Becker *et al.* [2014], which identified the presence of maximum setup at low tide, and a lower setup at high tide. Field measurements from a high energy fringing reef [Vetter *et al.*, 2010] and low energy reef platform [Jago *et al.*, 2007] have found that, on average, setup is 25% of H_o (incident H_o). Mean setup at the shoreline on Funafuti was 15.6% of H_o across all tides. However, setup at low tide ranged from 16.8% to 42% of H_o (mean = 28%), and at high tide setup ranged from 0% to 16.2% of H_o (mean = 6.2%). Similar tidal controls and incident wave height scaling were observed on atoll reefs in the Marshall Islands [Becker *et al.*, 2014].

Field results from Funafuti indicate that there is minimal tidal influence on IG wave activity at the reef flat or shoreline (Figure 3). Results show that H_{ig} increases between the reef flat and shoreline and suggest that IG waves are primarily a function of incident wave conditions; not reef flat water level. At Funafuti, H_{ig} at the shoreline scales between 10% and 43% of H_o (mean = 26%), with no clear tidal control (Figure 3). Results from Majuro Atoll, on a reef with similar morphology and wave exposure to Funafuti, also show H_{ig} at the shoreline to be between 10% and 40% of H_o [Ford *et al.*, 2013]. On the narrow reefs (~ 100 m) at Funafuti and Majuro, IG wave height was measured to increase across the reef flat and peak at the shoreline. IG waves were also measured to increase in height across a wider (~ 250 m) and relatively smooth reef on Kwajalein Atoll [Quataert *et al.*, 2015]. However, measurements on wide fringing reefs (+400 m) typically show IG wave height and energy peaks within ~ 100 m of the reef edge before dissipating across the reef flat to be minimal at the shoreline [Péquignet *et al.*, 2014; Pomeroy *et al.*, 2012]. Pronounced tidal controls on IG wave height have also been observed on wider fringing reefs, due to frictional dissipation across the inner reef flat [Van Dongeren *et al.*, 2013]. Given the location of Fatato Island relative to the reef edge, IG waves are able to impact the shoreline before any dissipation is observed.

6.2. Model Capability

The majority of phase-resolving model work on reefs has focused on continental fringing reefs, not atoll reefs that host low lying sedimentary islands [Nwogu and Demirbilek, 2010; Shimozono *et al.*, 2015; Yao *et al.*, 2012; Zijlema, 2012]. Such Boussinesq-type models have been shown to accurately replicate wave attenuation, wave setup, and IG wave dynamics when evaluated against wave flume data. Few phase-resolving models have been evaluated using field data from fringing or atoll reefs [Demirbilek and Nwogu, 2007; Roeber and Cheung, 2012]. Model results from Funafuti show that the Basilisk GN solver is capable of representing the key processes that contribute to elevated water depth at the shoreline. Water level dynamics associated with SS wave attenuation and wave setup were represented with skill >0.97 and mean error <0.045 m. IG wave dynamics were also represented reasonably well, with skill = 0.91. Wave height and setup predictions were slightly sensitive to breaking and friction parameters, whereas IG wave heights were highly sensitive to low B values and high friction.

Using measured water level data as a boundary wave condition assisted in achieving a skilful representation of measured processes at the reef flat and shoreline. Using the measured incident wavefield for each burst allowed the model to generate a close representation of IG wave motions and setup dynamics. Using a parametric wavefield from a JONSWAP spectrum with the same incident wave statistics would result in similar, but not identical wave processes at the shoreline. It is evident that a monochromatic wavefield would result in over-predicted setup and under-represented IG waves. The dynamic representation of IG waves and setup achieved using Basilisk GN support the results from Roeber and Bricker [2015] that highlight the benefits of using a phase-resolving model when investigating wave dynamics and inundation on reef coastlines.

Limitations to the model results cannot be overlooked. While wave transformation results were tested against field data, no data were available to confirm model predictions of R_{max} . However, the Basilisk GN model has been tested against benchmark runup scenarios [Popinet, 2014], that give some confidence to R_{max} values. Beach porosity and percolation were also not accounted for in runup estimations, possibly resulting in overpredicted runup levels. Further, as the model was used in 1-D, omitting alongshore processes that influence wave transformation and runup (e.g., refraction, wave convergence, alongshore currents, and edge waves) were omitted. Using the model in 2-D would allow variations in incident wave direction and across shore bathymetry to be represented. However, the higher computational cost of running the model in 2-D significantly limits the number of simulations that can be used for model evaluation and analysis.

6.3. Maximum Shoreline Runup

The unconsolidated sedimentary structure and low elevation make atoll islands susceptible to wave overtopping and erosion during high energy wave events or periods of elevated sea level [Hoeke et al., 2013]. An understanding of the processes that contribute to increased wave interactions with the shoreline is critical for coastal management, and to mitigate the potentially adverse effects of future sea level rise on atoll landforms [Ferrario et al., 2014]. Recent research has highlighted that wave driven flooding can be caused by long period swell waves which are generated by distant weather systems [Hoeke et al., 2013]. However, large waves typically need to coincide with high tide for overtopping to occur. Merrifield et al. [2014] show that overtopping events happen every 2–5 years in the Marshall Islands but will occur multiple times per year with any rise in mean sea level greater than 0.4 m. Results from Merrifield et al. [2014] indicate that, on average, 52% of nontidal water level was a result of wave setup, with a further 48% associated with SS or IG waves. An overtopping event was also measured by Ford et al. [2013] on Majaro Atoll, where land elevation was 2 m above the reef flat. Overwash was generated by 2 m incident waves at high tide and was primarily driven by energetic IG waves at the shoreline ($H_{ig} = 0.8$ m), with a low contribution from SS waves and setup ($H_{ss} = 0.4$ m, $\bar{\eta} \approx 0.2$ m).

The analysis presented here extends the current understanding of wave interactions with atoll islands by focusing on the processes that promote wave interaction with the beach face. Results provide the first assessment of wave processes impacting islands on Funafuti Atoll, where sea level is currently rising at 3 times the global average rate [Becker et al., 2012]. Funafuti Atoll is also characterized by a narrow reef flat and steep fore-reef slope (23.5°), which according to Quataert et al. [2015] increases the risk of wave driven flooding when exposed to a rise in mean sea level. The elevated ocean berm on Fatato prevented any overtopping events, but results do highlight the temporal nature of wave processes that operate on the beach face. Significantly, IG waves are identified as having the dominant influence on runup elevation (41%), compared to wave setup (27.4%), and SS waves (31.6%). However, it is apparent that the runup mode shifts through the tide cycle. At low tide, SS wave height is significantly dissipated (78%), and IG wave activity is slightly limited by spring low tides and higher friction. Wave setup is at a maximum at low tide and provides the main control on shoreline water level, along with a significant presence of IG wave height. At midtide, larger SS waves propagate across the reef flat, setup decreases, and IG waves control runup elevation. At high tide, wave runup is driven by a combination of SS and IG waves, with a small contribution from wave setup.

6.4. Island Exposure to Wave Processes

The beach face on Fatato Island is located 0.39 m above MSL. Using field measurements, tide level exceeded the beach toe elevation for 22.4% of the experiment. Tide station data from the atoll lagoon also show that tides above +0.39 m occur for 23% of the year. Mean water depth at the shoreline (tide + setup) exceeded beach toe elevation for 25% of the experiment. These results suggest the beach face was directly exposed to wave activity for a quarter of the experimental period. However, model analysis of maximum runup as a function of SS waves, IG waves, setup, and tide level reveal that waves actually impacted at or above the beach toe for 70.8% of the deployment, with wave activity on the midbeach face for 57.4% of the experiment.

Modeled R_{max} results show that islands on the south-eastern rim of Funafuti are much more connected to ocean processes than topographic and tide measurements suggest. Geomorphic change on atoll islands is limited to the temporal window of island exposure to wave activity [Kench and Brander, 2006]. By measuring depth controls on SS wave propagation across different reef flats Kench and Brander [2006] show that interaction between wave processes and island shorelines is limited to a small temporal window at high tide. Results from Funafuti highlight the importance of accounting for water level oscillations at all surf-zone frequencies when assessing wave impacts at the shoreline. Accounting for R_{max} significantly increases the

temporal window of connectivity between wave processes and island sediment on Funafuti. Under typical wave conditions, sediment transport between the reef flat and island beach can occur for the majority of the tide cycle (71%). However, when exposed to higher wave energy, the island can be connected to wave activity for the entire tide cycle. The enhanced interaction between waves and the island is attributed to the large setup at low tide that results in IG wave activity on the reef flat at all tide stages. The narrow reef flat also results in IG waves impacting the island without any dissipation or tidal forcing being observed in field or model data. Results suggest that even a small rise in sea level may result in waves reaching the shoreline for the complete tide cycle, significantly increasing the period of time when geomorphic change can occur on the beach face.

7. Summary

Field data collected from a 62 day deployment were examined to understand wave transformation on Funafuti Atoll and evaluate a numerical models capability of simulating SS wave attenuation, IG wave behavior and wave setup. Research from Funafuti indicates that the island shoreline is highly connected to wave processes, despite sitting 0.39 m above MSL and only being submerged for 23% of the tide cycle. Tidal level has a strong control on SS waves and wave setup at the shoreline on Fatato Island. Therefore, SS waves have the primary influence on runup elevation at high tide and wave setup largely determines runup elevation at low tide. Field and model results indicate that infragravity wave activity is not tidally modulated on Funafuti, and runup analysis show IG waves are capable of elevating shoreline water level throughout the tide cycle. Tide level and setup, combined with runup from SS and IG waves resulted in swash reaching island sediment for 71% of the deployment. This is a much longer window for geomorphic activity than identified only using tide data which suggest a 23% temporal window for geomorphic change. The increase in setup and IG wave activity during swell events mean that waves can interact with the beach face for a complete spring tide cycle. These results imply that any rise in sea level will further increase the temporal window of interaction between waves and island sediment, with SS and IG waves becoming the dominant processes influencing shoreline water level.

Acknowledgments

The Basilisk model is freely available from basilisk.fr. Field data, simulation files, model input data, and output data can be made available to anyone who contacts the corresponding author (e.beetham@auckland.ac.nz). This research is part of a PhD thesis being undertaken by Eddie Beetham at the University of Auckland (UoA), supported by a UoA Doctoral scholarship. Field data were collected in conjunction with Secretariat of the Pacific Community (SPC) GeoScience division (Suva, Fiji) as part of the WACOP (Waves and Coasts in the Pacific) project funded by the European Union, grant FED/2011/281-131. Special thanks to Jens Kruger and Cyprien Bosserelle at SPC GeoScience for organizing the collaborative research. We would also like to thank Ron Hoeke at CSIRO (Melbourne, Australia) for providing bathymetric and wave hindcast data. Finally, thank you to Giovanni Coco (UoA) for helpful feedback and discussions.

References

- Audusse, E., F. Bouchut, M. O. Bristeau, R. Klein, and B. Perthame (2004), A fast and stable well-balanced scheme with hydrostatic reconstruction for vs hallow water flows, *SIAM J. Sci. Comput.*, 25(6), 2050–2065.
- Becker, J., M. Merrifield, and M. Ford (2014), Water level effects on breaking wave setup for Pacific Island fringing reefs, *J. Geophys. Res. Oceans*, 119, 914–932, doi:10.1002/2013JC009373.
- Becker, M., B. Meyssignac, C. Letetrel, W. Llovel, A. Cazenave, and T. Delcroix (2012), Sea level variations at tropical Pacific islands since 1950, *Global Planet. Change*, 80–81, 85–98, doi:10.1016/j.gloplacha.2011.09.004.
- Bonneton, P., F. Chazel, D. Lannes, F. Marche, and M. Tissier (2011), A splitting approach for the fully nonlinear and weakly dispersive Green-Naghdi model, *J. Comput. Phys.*, 230(4), 1479–1498, doi:10.1016/j.jcp.2010.11.015.
- Brander, R. W., P. S. Kench, and D. Hart (2004), Spatial and temporal variations in wave characteristics across a reef platform, Warraber Island, Torres Strait, Australia, *Mar. Geol.*, 207(1–4), 169–184, doi:10.1016/j.margeo.2004.03.014.
- Demirbilek, Z., and O. G. Nwogu (2007), Boussinesq modeling of wave propagation and runup over fringing coral reefs, model evaluation report, Rep. ERDC/CHL TR-07-12, U.S. Army Eng. Res. and Dev. Cent., Washington, D. C.
- Durrant, T., D. Greenslade, H. Hemer, and C. Trenham (2014), A global wave hindcast focussed on the Central and South Pacific, CAWCR Tech. Rep. 070, Bureau of Meteorology, Melbourne, Australia.
- Ferrario, F., M. W. Beck, C. D. Storlazzi, F. Micheli, C. C. Shepard, and L. Airoldi (2014), The effectiveness of coral reefs for coastal hazard risk reduction and adaptation, *Nat. Commun.*, 5, 3794, doi:10.1038/ncomms4794.
- Ford, M., J. Becker, and M. Merrifield (2013), Reef flat wave processes and excavation pits: Observations and implications for Majuro Atoll, Marshall Islands, *J. Coastal Res.*, 29(3), 545–554, doi:10.2112/jcoastres-d-12-00097.1.
- Gourlay, M. R. (1996), Wave set-up on coral reefs. 1: Set-up and wave-generated flow on an idealised two dimensional horizontal reef, *Coastal Eng.*, 27(3–4), 161–193.
- Hearn, C. J. (1999), Wave-breaking hydrodynamics within coal reef systems and the effect of changing relative sea level, *J. Geophys. Res.*, 104(12), 30,007–30,019.
- Hoeke, R., K. L. McInnes, J. C. Kruger, R. J. McNaught, J. R. Hunter, and S. G. Smithers (2013), Widespread inundation of Pacific islands triggered by distant-source wind-waves, *Global Planet. Change*, 108, 128–138, doi:10.1016/j.gloplacha.2013.06.006.
- Hoeke, R., K. McInnes, and J. O'Grady (2014), Downscaling wave climate at a Funafuti, Tuvalu, report, Cent. for Aust. Weather and Clim. Res., Melbourne, Australia.
- Jago, O. K., P. S. Kench, and R. W. Brander (2007), Field observations of wave-driven water-level gradients across a coral reef flat, *J. Geophys. Res.*, 112, C06027, doi:10.1029/2006JC003740.
- Kench, P. S., and R. W. Brander (2006), Wave processes on coral reef flats: Implications for reef geomorphology using Australian case studies, *J. Coastal Res.*, 22(1), 209–223, doi:10.2112/05a-0016.1.
- Lannes, D., and F. Marche (2015), A new class of fully nonlinear and weakly dispersive Green-Naghdi models for efficient 2D simulations, *J. Comput. Phys.*, 282, 238–268, doi:10.1016/j.jcp.2014.11.016.
- Lin, C. C., C. R. Ho, and Y. H. Cheng (2014), Interpreting and analyzing King Tide in Tuvalu, *Nat. Hazards Earth Syst. Sci.*, 14(2), 209–217, doi:10.5194/nhess-14-209-2014.

- Lowe, R. J., J. L. Falter, S. G. Monismith, and M. J. Atkinson (2009), A numerical study of circulation in a coastal reef-lagoon system, *J. Geophys. Res.*, 114, C06022, doi:10.1029/2008JC005081.
- Lugo-Fernandez, A., H. H. Roberts, and W. J. Wiseman (1998), Tide effects on wave attenuation and wave set-up on a Caribbean coral reef, *Estuarine Coastal Shelf Sci.*, 47(4), 385–393.
- Maragos, J. E., and P. J. Beveridge (1973), Tropical cyclone bebe creates a new land formation on Funafuti Atoll, *Science*, 181(4105), 1161–1164.
- Merrifield, M., J. Becker, M. Ford, and Y. Yao (2014), Observations and estimates of wave-driven water level extremes at the Marshall Islands, *Geophys. Res. Lett.*, 41, 7245–7253, doi:10.1002/2014GL061005.
- Nwogu, O., and Z. Demirbilek (2010), Infragravity wave motions and runup over shallow fringing reefs, *J. Waterw. Port Coastal Ocean Eng.*, 136(6), 295–305.
- Péquignet, A. C., J. M. Becker, M. A. Merrifield, and S. J. Boc (2011), The dissipation of wind wave energy across a fringing reef at Ipan, Guam, *Coral Reefs*, 30(1), 71–82, doi:10.1007/s00338-011-0719-5.
- Péquignet, A. C., J. M. Becker, and M. A. Merrifield (2014), Energy transfer between wind waves and low-frequency oscillations on a fringing reef, Ipan, Guam, *J. Geophys. Res. Oceans*, 119, 6709–6724, doi:10.1002/2014JC010179.
- Pomeroy, A., R. Lowe, G. Symonds, A. Van Dongeren, and C. Moore (2012), The dynamics of infragravity wave transformation over a fringing reef, *J. Geophys. Res.*, 117, C11022, doi:10.1029/2012JC008310.
- Popinet, S. (2011), Quadtree-adaptive tsunami modelling, *Ocean Dyn.*, 61(9), 1261–1285, doi:10.1007/s10236-011-0438-z.
- Popinet, S. (2012), Adaptive modelling of long-distance wave propagation and fine-scale flooding during the Tohoku tsunami, *Nat. Hazards Earth Syst. Sci.*, 12(4), 1213–1227, doi:10.5194/nhess-12-1213-2012.
- Popinet, S. (2014), A solver for the Green-Naghdi equations, Basilisk, Paris, France. [Available at <http://www.basilisk.fr/src/green-naghdi.h>.]
- Popinet, S. (2015), A quadtree-adaptive multigrid solver for the Serre–Green–Naghdi equations, *J. Comput. Phys.*, 302, 336–358, doi:10.1016/j.jcp.2015.09.009
- Quataert, E., C. Storlazzi, A. van Rooijen, O. Cheriton, and A. van Dongeren (2015), The influence of coral reefs and climate change on wave-driven flooding of tropical coastlines, *Geophys. Res. Lett.*, 42, 6407–6415, doi:10.1002/2015GL064861.
- Roeber, V., and J. D. Bricker (2015), Destructive tsunami-like wave generated by surf beat over a coral reef during Typhoon Haiyan, *Nat. Commun.*, 6, 7854, doi:10.1038/ncomms8854.
- Roeber, V., and K. F. Cheung (2012), Boussinesq-type model for energetic breaking waves in fringing reef environments, *Coastal Eng.*, 70, 1–20.
- Ryan, E. (2012), The nearshore process regime around an atoll motu and implications for beach morphodynamics: A case study of Fatato, Funafuti Atoll, Tuvalu, Masters thesis, 147 pp., Sch. of Environ., Univ. of Auckland, Auckland, New Zealand.
- Shimozono, T., Y. Tajima, A. B. Kennedy, H. Nobuoka, J. Sasaki, and S. Sato (2015), Combined infragravity wave and sea-swell runup over fringing reefs by super typhoon Haiyan, *J. Geophys. Res. Oceans*, 120, 4463–4486, doi:10.1002/2015JC010760.
- Tissier, M., P. Bonneton, F. Marche, F. Chazel, and D. Lannes (2012), A new approach to handle wave breaking in fully non-linear Boussinesq models, *Coastal Eng.*, 67, 54–66, doi:10.1016/j.coastaleng.2012.04.004.
- Tucker, M. J., and E. G. Pitt (2001), Waves in Ocean Engineering, Ocean Eng. Book Ser., vol. 5, 521 pp., Elsevier, N. Y.
- Van Dongeren, A., R. Lowe, A. Pomeroy, D. M. Trang, D. Roelvink, G. Symonds, and R. Ranasinghe (2013), Numerical modeling of low-frequency wave dynamics over a fringing coral reef, *Coastal Eng.*, 73, 178–190, doi:10.1016/j.coastaleng.2012.11.004.
- Vetter, O., J. M. Becker, M. A. Merrifield, A. C. Péquignet, J. Aucan, S. J. Boc, and C. E. Pollock (2010), Wave setup over a Pacific Island fringing reef, *J. Geophys. Res.*, 115, C12066, doi:10.1029/2010JC006455.
- Welch, P. (1967), The use of fast Fourier transform for the estimation of power spectra: A method based on time averaging over short, modified periodograms, *Audio and Electroacoustics, IEEE Transactions on*, 15(2), 70–73.
- Woodroffe, C. D. (2008), Reef-island topography and the vulnerability of atolls to sea-level rise, *Global Planet. Change*, 62(1–2), 77–96, doi:10.1016/j.gloplacha.2007.11.001.
- Yamano, H., H. Kayanne, T. Yamaguchi, Y. Kuwahara, H. Yokoki, H. Shimazaki, and M. Chikamori (2007), Atoll island vulnerability to flooding and inundation revealed by historical reconstruction: Fongafale Islet, Funafuti Atoll, Tuvalu, *Global Planet. Change*, 57(3–4), 407–416, doi:10.1016/j.gloplacha.2007.02.007.
- Yao, Y., Z. Huang, S. G. Monismith, and E. Y. M. Lo (2012), 1DH Boussinesq modeling of wave transformation over fringing reefs, *Ocean Eng.*, 47, 30–42.
- Zijlema, M. (2012), Modelling wave transformation across a fringing reef using swash, *Coastal Eng. Proc.*, 1(33), doi:10.9753/icce.v33.currents.26.